Available online at www.sciencedirect.com
SCIENCE DIRECT®
Journal of Solid State Chemistry 175 (2003) 237–244
JOURNAL OF SOLID STATE CHEMISTRY
http://elsevier.com/locate/jssc

Superconductivity and crystal structure of the solid solutions of $Ba_{8-\delta}Si_{46-x}Ge_x$ ($0 \leqslant x \leqslant 23$) with Type I clathrate structure

Hiroshi Fukuoka,* Junichi Kiyoto, and Shoji Yamanaka

Department of Applied Chemistry, Graduate School of Engineering, Hiroshima University, Higashi-Hiroshima 739-8527, Japan

Received 10 January 2003; received in revised form 26 April 2003; accepted 6 May 2003

Abstract

The solid solutions of barium containing Type I clathrate, $Ba_{8-\delta}Si_{46-x}Ge_x$ ($0 \leqslant x \leqslant 23$) were prepared under high-pressure and high-temperature conditions of 3 GPa at 800°C. All the solid solutions showed superconductivity, and the transition temperature (T_c) decreased from 8.0 to 2.0 K as the germanium content increased from $x = 0$ to 23 in $Ba_{8-\delta}Si_{46-x}Ge_x$. The single crystals with five different compositions were obtained and the structures, compositions, and site occupancies were determined from X-ray single-crystal analysis. A slight barium deficiency was observed at Ba1 (2*a*) sites for all the clathrates. The Ge atoms replaced the Si atoms at the Si3 (24*k*) site in the composition range of $x < 8$, and then at the Si2 (16*i*) site. The crystals had a slight deficiency in the covalent (Si, Ge) network and the deficiency increased with the increase of the Ge content.

Keywords: Silicon clathrate; Superconductivity; Superconductor; Type I clathrate; Single-crystal analysis

1. Introduction

Since the discovery of superconductivity in Ba containing silicon clathrate compounds, $(Na,Ba)_xSi_{46}$, with a transition temperature (T_c) of about 4 K [1,2], much interest has been renewed to the Type I silicon clathrate compounds. The first Type I silicon clathrate compound Na_8Si_{46} was prepared from the thermal decomposition of NaSi by Kasper et al. [3,4]. The superconducting clathrate compounds were prepared by a similar thermal decomposition of the solid solutions between $BaSi_2$ and NaSi [1,2]. The Type I silicon clathrate is composed of face-sharing Si_{20} dodecahedra (@Si_{20}) and Si_{24} tetrakaidecahedra (@Si_{24}) as shown in Fig. 1 [3,4]. The sodium and barium atoms in $(Na,Ba)_xSi_{46}$ are located in these polyhedra. Recently, we have succeeded in the synthesis of a binary silicon clathrate $Ba_{8-\delta}Si_{46}$ by the reaction of $BaSi_2$ and Si under high-pressure and high-temperature (HPHT) conditions of 3 GPa and 800°C [5]. The compound showed superconductivity with $T_c = 8.0$ K. Theoretical studies of the electronic structure of this clathrate showed that Ba 5*d* states strongly hybridized with the Si_{46} host lattice states giving a sharp band near the Fermi level (E_F) [6–10]. The existence of such a sharp band was observed in the measurement of ultrahigh-resolution photoemission spectroscopy of $Ba_{8-\delta}Si_{46}$ [11].

In contrast to the superconducting $Ba_{8-\delta}Si_{46}$, a germanium analogue Ba_8Ge_{43} has Ge vacancies at the 6*c* sites [12,13], and is reported to be a semiconductor [12,13]. The remarkable difference in electrical properties between the silicon and germanium analogs is an interesting issue of the clathrate system. The formation of one vacancy in the framework may trap four electrons to form lone pairs on the four neighboring atoms of the vacancy. The electron carrier density, therefore, decreases and this would be the reason for the non-metallic properties of the germanium clathrate.

In the present study, we have prepared the solid solutions of $Ba_{8-\delta}Si_{46-x}Ge_x$ ($0 \leqslant x \leqslant 23$) to investigate the effect of the Ge substitution in the Si framework on the superconducting properties. Some ternary single crystals have been obtained, and the X-ray single-crystal studies have been made. The superconductivity is discussed in relation with the composition.

*Corresponding author. Fax: +81-824-24-5494.
E-mail address: hfukuoka@hiroshima-u.ac.jp (H. Fukuoka).

0022-4596/03/$ - see front matter © 2003 Elsevier Inc. All rights reserved.
doi:10.1016/S0022-4596(03)00253-6

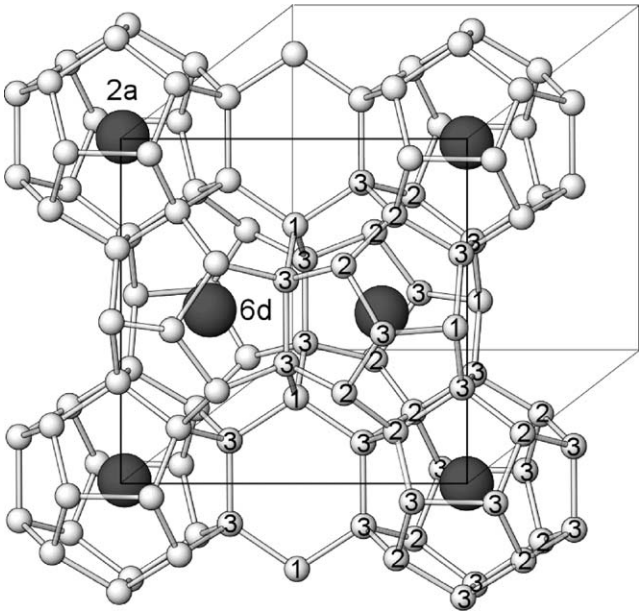

Fig. 1. Crystal structure of $Ba_{8-\delta}Si_{46}$ Type I clathrate. Only the polyhedra for the front face are shown. Small open and black solid balls represent Si and Ba atoms, respectively. The numbers 1, 2, and 3 in the open balls represent Si1(6*c*), Si2(16*i*), and Si3(24*k*) sites, respectively. The Ba 2*a* and 6*d* sites are located at the centers of Si_{20} dodecahedra (@Si_{20}) and Si_{24} tetrakaidecahedra (@Si_{24}), respectively.

2. Experimental

2.1. Preparation of clathrate compounds

Silicon (Katayama Chemical 99.9%) blocks and barium metal (Katayama Chemical 99%) were mixed in an atomic ratio of 2:1, and arc-melted under Ar atmosphere to obtain barium disilicide $BaSi_2$. $BaGe_2$ were prepared in a similar way from a mixture of Ba and Ge (Katayama Chemical 99.999%). Polycrystalline samples of $Ba_{8-\delta}Si_{46-x}Ge_x$ ($0 \leqslant x \leqslant 27$) were prepared from the mixtures of $BaSi_2$, $BaGe_2$, Si and Ge powders with different compositions. The mixtures were placed in h-BN cells (5 mm inner diameter and 5 mm length) in an Ar-filled glove box. Each BN cell was in turn placed in a carbon tube heater and packed in a pyrophyllite cube as pressure media. The cell was first compressed under a pressure of 3 GPa, and heated up to 800°C for 1 min. After standing at 800°C for 30 min, the cell was quickly cooled down to room temperature. Polycrystalline samples with silver metallic luster were obtained. These samples are hereafter called $Ba_8Si_{46-x}Ge_x$ ($0 \leqslant x \leqslant 27$) by their nominal compositions of the starting mixtures, although they may contain slight deficiencies on the Ba as well as (Si,Ge) sites.

2.2. Preparation of single crystals

Single crystals of the Ba–Si–Ge ternary clathrate compounds with different compositions were prepared using HPHT conditions. $BaSi_2$, $BaGe_2$, Si, and Ge powders were mixed in such a way that the nominal atomic ratios were $Ba_8Si_{41}Ge_5$, $Ba_8Si_{37}Ge_9$, and $Ba_8Si_{31}Ge_{15}$. Each mixture was placed in an h-BN cell (2.5 mm inner diameter and 6.5 mm length) in an Ar-filled glove box. The mixture was compressed under a pressure of 3 GPa and was heated up to 1000°C for 2 min, and then slowly cooled down to 700°C in 3 h, followed by quenching to room temperature. Single crystals with the Type I clathrate structure were obtained in association with small amounts of $BaSi_2$ and/or $BaGe_2$. The compositions of the single crystals were determined in the X-ray structure refinements.

Single crystals of $Ba_{8-\delta}Si_{46}$ were also prepared from a stoichiometric mixture of $BaSi_2$ and Si powder. The mixture was heated up to 1300°C for 2 min and then slowly cooled down to 800°C under a pressure of 3 GPa. Single crystals of Ba_8Ge_{43} were prepared using an arc furnace; germanium (Katayama Chemical 99.999%) and barium (Katayama Chemical 99%) were mixed in an atomic ratio of 8:43, and arc-melted under Ar atmosphere.

2.3. Characterization

All the polycrystalline clathrate samples were characterized by using a powder X-ray diffractometer (Mac Science, M18XHF) with graphite monochromated Cu*K*α radiation. Temperature dependence of the magnetic susceptibilities was measured using a SQUID magnetometer (Quantum Design MPMS-5) under a field of 5 Oe on zero field-cooled (ZFC) samples.

2.4. Structure analysis of single crystals

Single-crystal X-ray diffraction (XRD) data were collected with a Rigaku AFC7R diffractometer and a Rigaku RAXIS imaging plate area detector with monochromated Mo*K*α radiation. Rigaku TeXsan [14] and CrystalStructure crystallographic software package [15] were used in the structure refinement. The clathrate compounds crystallize in a cubic space group *Pm*-3*n*, and there are three crystallographically independent sites for Si atoms, Si1(6*c*), Si2(16*i*), and Si3(24*k*) as shown in Fig. 1.

In order to estimate the way of substitution of the Si sites with Ge, the structure refinement of the ternary clathrate compounds was performed in the following way. At first, a random-substitution model was assumed, in which all Si sites were randomly substituted with Ge atoms. In the refinement of the occupational factor of Ge atoms at each Si site, it was revealed that the single crystals with nominal compositions of $Ba_8Si_{41}Ge_5$ and $Ba_8Si_{37}Ge_9$ had the Ge substitution only at the 24*k* sites. A similar refinement made on the

single crystal $Ba_8Si_{31}Ge_{15}$ suggested that the Ge atoms substituted Si atoms on the 16*i* as well as the 24*k* sites.

In the next refinement, site deficiencies were examined, since the Ba containing binary Si clathrate Ba_8Si_{46} had Ba deficiency on the 2*a* site, and Ba_8Ge_{43} had Ge defects on the 6*c* site. When the occupational factors of the 2*a* and 6*c* sites were refined for the three ternary clathrates, the existence of deficiencies on both sites was suggested. Therefore, in the final refinement of $Ba_8Si_{41}Ge_5$ and $Ba_8Si_{37}Ge_9$, all parameters, including occupational parameters of the Ba1, Si1, Si3, and Ge3 sites, were refined together. In case of $Ba_8Si_{31}Ge_{15}$, all parameters including occupational parameters of the Ba1, Si1, Si2, Si3, Ge2, and Ge3 sites, were refined together. We calculated the compositions from the refined occupational factors and obtained the compositions of $Ba_{7.7}Si_{42.7}Ge_{3.1}$, $Ba_{7.7}Si_{39.3}Ge_{6.4}$, and $Ba_{7.9}Si_{33.3}Ge_{12.0}$ for crystals obtained from the nominal compositions of $Ba_8Si_{41}Ge_5$, $Ba_8Si_{37}Ge_9$, and $Ba_8Si_{31}Ge_{15}$, respectively.

The compositions of the single crystals were also determined using an electron probe microanalyzer. The compositions of the single crystals, $Ba_{7.7}Si_{42.7}Ge_{3.1}$ and $Ba_{7.9}Si_{33.3}Ge_{12.0}$ were determined to be $Ba_{7.2}Si_{42.0}Ge_{4.0}$ and $Ba_{7.9}Si_{32.9}Ge_{13.1}$, respectively. The two compositions obtained by the different methods are comparable within the accuracy of the analysis.

The crystal structure analysis of the single crystals Ba_8Si_{46} and Ba_8Ge_{43} were performed and the compositions of $Ba_{7.6}Si_{46}$ and $Ba_8Ge_{42.8}$ were obtained, respectively. The crystal structure of the germanium clathrate had already analyzed by Cabrera et al. [12,13]. They reported there was no deficiency on the barium sites. Cabrera et al. also reported a site splitting for Ge3 site, i.e. the Ge3 position split into two near sites. In our refinement, we examined the splitting structure model as well as the no-splitting model. The splitting model with 23 parameters gave the $R = 3.21\%$, $R_w = 2.36\%$, S (goodness of fit) $= 2.211$, and residual densities of $1.36/-1.14\,e\,Å^{-3}$, which showed no remarkable change from the results of no-splitting model with 16 parameters, $R = 3.69\%$, $R_w = 2.58\%$, $S = 2.397$, and $1.51/-1.31\,e\,Å^{-3}$. It is reasonable to conclude that our crystal did not show the clear splitting of the Ge3 site, because the splitting model did not improve the refinement considerably, even with a larger number of structure parameters used. The composition and the structural parameters obtained in this study were in good agreement with their results except for the splitting sites. This difference of the structure would be due to the difference of the synthesis methods. While we prepared the crystal using an arc furnace, they obtained the crystal by the decomposition of $Ba_3Ge_4C_2$ at 1123 K under a pressure of 40 kb.

Crystallographic data for these five single crystals are listed in Table 1. Atomic parameters and thermal vibrational parameters are listed in Tables 2 and 3. Selected bond distances are shown in Table 4.

3. Results and discussion

3.1. Solid solutions $Ba_8Si_{46-x}Ge_x$ and superconductivity

The powder XRD patterns of the typical ternary polycrystalline clathrate samples are shown in Fig. 2. The solid solutions of $Ba_8Si_{46-x}Ge_x$ clathrates were obtained as single phases in the composition range of $0 \leqslant x < 15$. In the range of higher germanium contents $x > 18$, weak reflection peaks due to silicon were observed as shown in Figs. 2d and e. The amounts of the Si impurity were estimated to be less than 3 wt% in

Table 1
Crystallographic data for clathrate single crystals with five different compositions

	Pm-3*n* (No.223)				
Formula	$Ba_{7.6}Si_{46}$	$Ba_{7.7}Si_{42.7}Ge_{3.1}$	$Ba_{7.7}Si_{39.3}Ge_{6.4}$	$Ba_{7.9}Si_{33.3}Ge_{12.0}$	Ba_8Ge_{43}
Space group					
a Å	10.331(2)	10.325(3)	10.3525(4)	10.4130(5)	10.660(2)
V Å^3	1102.8(2)	1100.6(4)	1109.52(6)	1129.09(9)	1212.0(4)
Crystal size (mm)	$0.10 \times 0.10 \times 0.05$	$0.20 \times 0.15 \times 0.05$	$0.25 \times 0.05 \times 0.05$	$0.15 \times 0.10 \times 0.15$	$0.15 \times 0.10 \times 0.03$
Diffractometer	Rigaku AFC 7R	Rigaku Rapid-Auto IP system	Rigaku Rapid-Auto IP system	Rigaku Rapid-Auto IP system	Rigaku AFC 7R
Radiation (graphite monochromated)		Mo$K\alpha$ 0.7107 Å			
Collection region (2θ limit)	$4 \leqslant 2\theta \leqslant 110$	$2\theta \leqslant 54.8$	$2\theta \leqslant 54.8$	$2\theta \leqslant 54.8$	$4 \leqslant 2\theta \leqslant 100$
No. of used reflections	480	201	214	186	335
No. of variable parameters	16	18	18	19	16
R, R_w[a]	0.023, 0.014	0.021, 0.009	0.015, 0.008	0.015, 0.013	0.037, 0.026
Residual density[b] (e Å^{-3})	0.69/−0.65	1.44/−0.95	0.61/−0.68	0.60/−0.86	1.51/−1.31

[a] $R(F_o) = \sum(||F_o| - |F_c||)/\sum|F_o|$, $R_w(F_o) = [\sum w(|F_o| - |F_c|)^2/\sum wF_o^2]^{1/2}$ ($w = 1/\sigma(F_o)^2$).
[b] The highest and lowest residual electrons of the final difference Fourier map.

Table 2
Atomic parameters for clathrate single crystals with five different compositions with standard deviations in parentheses

Atom	Site	x	y	z	B_{eq} (Å^2)	Ocp.
$Ba_{7.6}Si_{46}$						
Ba1	2*a*	0	0	0	0.851(2)	0.804(2)
Ba2	6*d*	0.25	0.5	0	1.353(4)	1
Si1	6*c*	0.25	0	0.5	0.94(1)	1
Si2	16*i*	0.18491(5)	0.18491	0.18491	0.807(2)	1
Si3	24*k*	0	0.30623(8)	0.12142(7)	0.88(1)	1
$Ba_{7.7}Si_{42.7}Ge_{3.1}$						
Ba1	2*a*	0	0	0	1.46(2)	0.856(5)
Ba2	6*d*	0.25	0.5	0	1.75(3)	1
Si1	6*c*	0.25	0	0.5	1.18(7)	0.963(7)
Si2	16*i*	0.18501(8)	0.18501	0.18501	1.10(1)	1
Si3	24*k*	0	0.3081(1)	0.1229(1)	1.35(3)	0.872(4)
Ge3	24*k*	0	0.3081	0.1229	1.35	0.128
$Ba_{7.7}Si_{39.3}Ge_{6.4}$						
Ba1	2*a*	0	0	0	1.14(1)	0.862(2)
Ba2	6*d*	0.25	0.5	0	1.73(1)	1
Si1	6*c*	0.25	0	0.5	1.29(5)	0.955(6)
Si2	16*i*	0.18478(6)	0.18478	0.18478	0.74(1)	1
Si3	24*k*	0	0.31146(7)	0.12329(7)	1.32(2)	0.734(2)
Ge3	24*k*	0	0.31146	0.12329	1.32	0.266
$Ba_{7.9}Si_{33.3}Ge_{12.0}$						
Ba1	2*a*	0	0	0	1.29(1)	0.936(5)
Ba2	6*d*	0.25	0.5	0	2.26(1)	1
Si1	6*c*	0.25	0	0.5	1.48(5)	0.880(8)
Si2	16*i*	0.18510(6)	0.18510	0.18510	1.30(2)	0.912(2)
Ge2	16*i*	0.18510	0.18510	0.18510	1.30	0.088
Si3	24*k*	0	0.31439(7)	0.12370(6)	1.78(2)	0.560(4)
Ge3	24*k*	0	0.31439	0.12370	1.78	0.440
Ba_8Ge_{43}						
Ba1	2*a*	0	0	0	1.121(5)	1
Ba2	6*d*	0.25	0.5	0	2.61(2)	1
Ge1	6*c*	0.25	0	0.5	1.13(5)	0.473(8)
Ge2	16*i*	0.18373(6)	0.18373	0.18373	1.331(3)	1
Ge3	24*k*	0	0.3195(1)	0.1213(1)	2.33(2)	1

these samples and the deviation of the composition from the nominal one must be very small. The lattice constant increased with the increase of the germanium content as shown in Fig. 3. The increase of the lattice constant with x is due to the larger covalent radius of germanium than that of silicon. Fig. 4 shows the temperature dependence of the magnetic susceptibility of the solid solutions. All the samples with $x<23$ showed magnetic transitions due to the onset of superconductivity. The transition temperature (T_c) decreased with the increase of Ge substitution as shown in Fig. 3 together with the change of the lattice constant.

3.2. Single-crystal structures

The single crystals of the solid solutions were not obtained as a single phase, but associated with small amounts of $BaSi_2$ and/or $BaGe_2$. The composition of each single crystal was determined by the refinements of the X-ray structural analysis. The plots of the lattice constants vs. compositions x obtained for the single crystals are given in Fig. 3. As can be seen, the plots fall on the curve for the powder solid solutions. It would be reasonable to conclude that the structures of the solid solutions are very similar to the structures of single crystals if the compositions or the lattice constants are the same. The host structure of the Type I silicon clathrate is constructed of Si_{20} and Si_{24} cages. The Si atoms of the Si_{20} cage are on the Si2(16*i*) and Si3(24*k*) sites. The Si atoms on the Si1(6*c*) sites are not included in the Si_{20} cages, but bridge Si_{20} cages. The Ba1(2*a*) and the Ba2(6*d*) sites are at the center of the Si_{20} and Si_{24} cages, respectively.

The site distributions of the elements in the unit cell of the clathrate solid solutions were calculated on the basis of the data given in Table 2, and shown as schematic diagrams in Fig. 5. The distributions of Si and Ge atoms in the network (Si1, Si2, and Si3 sites) and Ba atoms in

Table 3
Thermal vibrational parameters for clathrate single crystals with five different compositions with standard deviations in parentheses

Atom	U_{11}	U_{22}	U_{33}	U_{12}	U_{13}	U_{23}
$Ba_{7.6}Si_{46}$						
Ba1	0.0108(2)	0.0108	0.0108	0.0	0.0	0.0
Ba2	0.0163(2)	0.0176(2)	0.0176	0.0	0.0	0.0
Si1	0.0107(4)	0.0107	0.0141(7)	0.0	0.0	0.0
Si2	0.0102(1)	0.0102	0.0102	−0.0004(2)	−0.0004	−0.0004
Si3	0.0134(3)	0.0098(3)	0.0103(3)	0.0	0.0	0.0000(3)
$Ba_{7.7}Si_{42.7}Ge_{3.1}$						
Ba1	0.0185(5)	0.0185	0.0185	0.0	0.0	0.0
Ba2	0.0215(5)	0.0225(3)	0.0225	0.0	0.0	0.0
Si1	0.010(1)	0.010	0.026(2)	0.0	0.0	0.0
Si2	0.0139(4)	0.0139	0.0139	0.0005(5)	0.0005	0.0005
Si3(Ge3)	0.0130(7)	0.0187(7)	0.0196(8)	0.0	0.0	0.0020(7)
$Ba_{7.7}Si_{39.3}Ge_{6.4}$						
Ba1	0.0144(4)	0.0144	0.0144	0.0	0.0	0.0
Ba2	0.0198(4)	0.0229(3)	0.0229	0.0	0.0	0.0
Si1	0.009(1)	0.009	0.031(2)	0.0	0.0	0.0
Si2	0.0093(3)	0.0093	0.0093	0.0006(3)	0.0006	0.0006
Si3(Ge3)	0.0098(5)	0.0221(5)	0.0181(5)	0.0	0.0	0.0040(4)
$Ba_{7.9}Si_{33.3}Ge_{12.0}$						
Ba1	0.0164(3)	0.0164	0.0164	0.0	0.0	0.0
Ba2	0.0236(4)	0.0311(3)	0.0311	0.0	0.0	0.0
Si1	0.014(1)	0.014	0.028(2)	0.0	0.0	0.0
Si2(Ge2)	0.0165(4)	0.0165	0.0165	−0.0004(3)	−0.0004	−0.0004
Si3(Ge3)	0.0154(4)	0.0295(5)	0.0228(4)	0.0	0.0	0.0049(3)
Ba_8Ge_{43}						
Ba1	0.0142(3)	0.0142	0.0142	0.0	0.0	0.0
Ba2	0.0211(7)	0.0390(6)	0.0390	0.0	0.0	0.0
Ge1	0.017(2)	0.013	0.013(3)	0.0	0.0	0.0
Ge2	0.0169(2)	0.0169	0.0169	−0.0025(3)	−0.0025	−0.0025
Ge3	0.0169(5)	0.0410(7)	0.0306(6)	0.0	0.0	0.0168(6)

Table 4
Selected and average bond distances (Å) of the clathrate single crystals with five different compositions

	$Ba_{7.6}Si_{46}$	$Ba_{7.7}Si_{42.7}Ge_{3.1}$	$Ba_{7.7}Si_{39.3}Ge_{6.4}$	$Ba_{7.9}Si_{33.3}Ge_{12.0}$	$Ba_8Ge_{42.8}$
Si2–Si2	2.330(2)	2.324(3)	2.339(2)	2.341(2)	Ge2–Ge2 2.447(2)
Si3–Si3	2.509(1)	2.539(2)	2.553(1)	2.576(1)	Ge3–Ge3 2.587(3)
Si2–Si3	2.3772(5)	2.382(1)	2.405(1)	2.436(1)	Ge2–Ge3 2.5253(9)
Si1–Si3	2.4024(7)	2.377(1)	2.352(1)	2.338(1)	Ge1–Ge3 2.363(1)
$Si1_{ave}$[a]	2.402	2.377	2.352	2.338	$Ge1_{ave}=2.363$
$Si2_{ave}$[a]	2.365	2.368	2.389	2.412	$Ge2_{ave}=2.506$
$Si3_{ave}$[a]	2.416	2.420	2.429	2.447	$Ge3_{ave}=2.500$
$Ba1_{ave}$[b]	3.366	3.379	3.406	3.446	$Ba1_{ave}=3.543$
$Ba2_{ave}$[b]	3.7124	3.706	3.710	3.726	$Ba2_{ave}=3.8104$

[a] Averaged Si–Si distances of each Si site.
[b] Averaged Ba–Si distances of each Ba site.

the cages (Ba1 and Ba2 sites) are shown separately. Each partition in the bars corresponds to the five crystallographically independent sites and the length represents the number of atoms occupying on each site in a unit cell. The hatched areas in the 24*k* and 16*i* sites show the distribution of substituted Ge atoms. It is clearly shown that in the early stage of Ge substitution, Ge atoms predominantly substitute Si atoms on the Si3(24*k*) sites. After half of the Si3 sites are replaced with Ge atoms, the additional Ge atoms occupy the Si2(16*i*) sites. The Si1 (6*c*) site was not substituted with Ge atoms.

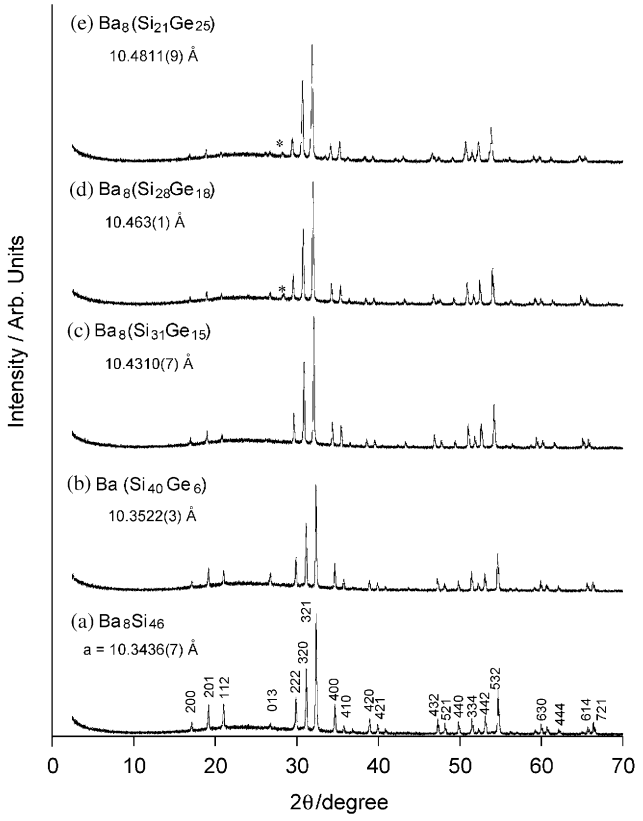

Fig. 2. Powder XRD patterns for the solid solutions of $Ba_8Si_{46-x}Ge_x$. (a) Ba_8Si_{46}, (b) $Ba_8(Si_{40},Ge_6)$, (c) $Ba_8(Si_{31},Ge_{15})$, (d) $Ba_8(Si_{28}Ge_{18})$, and (e) $Ba_8(Si_{21},Ge_{25})$. * Indicates a reflection of Si.

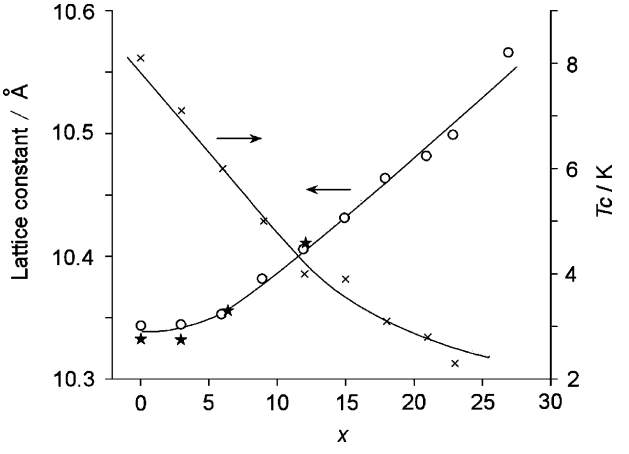

Fig. 3. The lattice constant (○) and the T_c (×) of the solid solutions as a function of Ge content x in $Ba_8Si_{46-x}Ge_x$. The lattice constants vs. the compositions determined by the refinements using the single crystals (★) are shown together in the same figure.

In the clathrate structure, each silicon site is tetrahedrally bonded to four (Si, Ge) atoms. The average value of the four bond distances can be a measure of the size of each Si site at the center of the tetrahedron. The average bond distances of the three kinds of Si sites are shown in Table 4. The average Ba–Si(Ge) bond distances in the dodecahedral ($Ba1_{ave}$) and

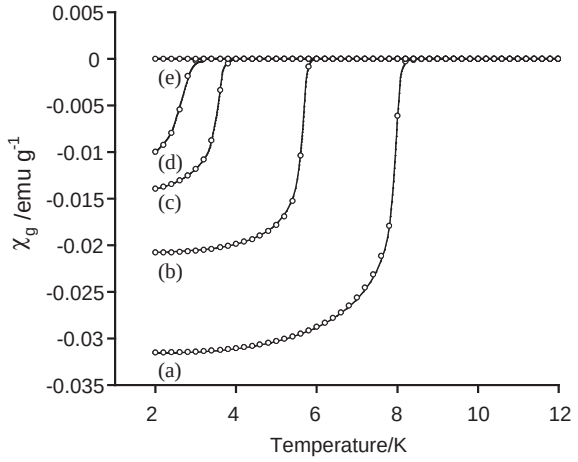

Fig. 4. Temperature dependences of the magnetic susceptibility of the solid solutions of $Ba_8Si_{46-x}Ge_x$. (a) Ba_8Si_{46}, (b) $Ba_8(Si_{40},Ge_6)$, (c) $Ba_8(Si_{31},Ge_{15})$, (d) $Ba_8(Si_{28},Ge_{18})$, (e) $Ba_8(Si_{23},Ge_{23})$.

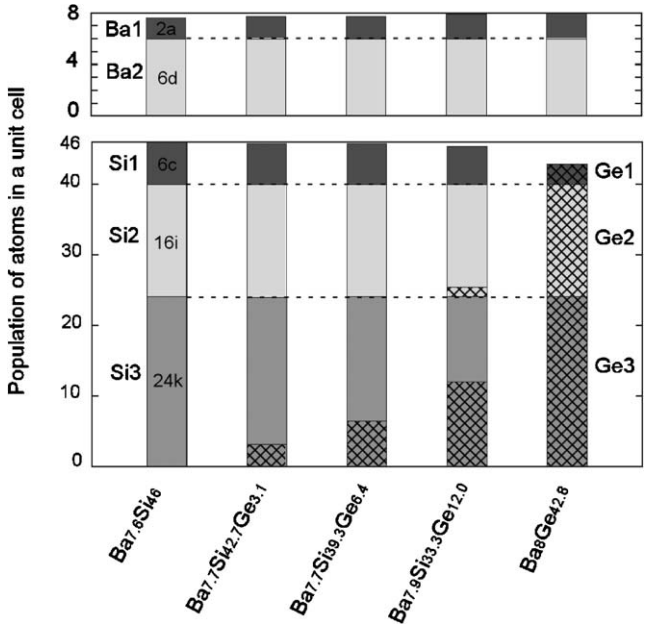

Fig. 5. Populations of Si, Ge, and Ba atoms in the unit cell of the five single crystals with different compositions. The hatched area show the distribution of Ge atoms in the Si sites.

tetrakaidecahedral ($Ba2_{ave}$) cages are similarly calculated, and given in Table 4. The site preference of Ge atoms appears to be related to the size of the Si sites. The Si3 site is the largest among the three kinds of Si sites in $Ba_{7.6}Si_{46}$, and could be preferentially replaced by Ge atoms. The distances of the Si3–Si3 and Si2–Si3 of bonds shown in Table 4 increased monotonically with the increase of Ge content, while the distance of the Si2–Si2 bonds which are not concerned with the formation of the dodecahedral cages showed essentially no change from the value of $Ba_{7.6}Si_{46}$. These findings are consistent with the fact that the substitution of Ge occurs on the Si3 (24*k*) site first. As can be seen from Fig. 3, the lattice

constants of the solid solutions were almost constant in the composition range of $x<10$, and then increased with increase of Ge content. This finding may reflect the shift of the Ge substitution sites from the 24*k* to 16*i* sites.

Two different types of defects were observed on the Si1(6*c*) and Ba1(2*a*) sites. The defect of Si atoms was observed only on the Si1(6*c*) site. The one end member of the system $Ba_8Ge_{42.8}$ had ca. 50% deficiency in the Ge1(6*c*) sites. Note that the bond length of Si1–Si3 decreased with the increase of the Ge substitution, and the bond length of Ge1–Ge3 was shorter than that of Si1–Si3 in Ba_8Si_{46}. This decrease would be explained in terms of the formation of defects on the 6*c* site. $Ba_{7.6}Si_{46}$ and $Ba_{7.7}Si_{42.7}Ge_{3.1}$ had no or very small amount of vacancies on the Si1 site and, therefore, the Ge1–Ge3 distance was smaller than the Si1–Si3 distances in these compounds. On the other hand, $Ba_{7.7}Si_{39.3}Ge_{6.4}$ and $Ba_{7.9}Si_{33.3}Ge_{12.0}$ had the shorter Si1–Si3 distances than that in $Ba_8Ge_{42.8}$ since they had many vacancies on the Si1 site compared to $Ba_{7.7}Si_{42.7}Ge_{3.1}$.

All the crystals except for $Ba_8Ge_{42.8}$ had a Ba deficiency on the Ba1(2*a*) site. The amount of Ba deficiency decreased with the increase of Ge contents. The reason of the formation of the defect on the Ba1 site is not known. One possible reason would be related with the large atomic radius of Ba. The Si_{20} cages in Type I structure appear to be tight for large Ba atoms (Table 4). This estimation will be supported by the fact that the sodium containing clathrate can be prepared under an ambient pressure but the binary barium clathrate can be obtained only by using HTHP conditions. The deficiency of Ba1(2*a*) site decreased with the increase of Ge content and in $Ba_8Ge_{42.8}$ there is no defect on the site. This is due to the expansion of the Si_{20} cages by the Ge substitution.

3.3. Superconductivity

The T_c gradually decreased from 8.0 K for $Ba_{7.6}Si_{46}$ to 2.2 K for $Ba_{8-\delta}Si_{23}Ge_{23}$ with the increase of the Ge content. The effects of the Ge substitution on the clathrate structure are: (i) to increase of the lattice constant, (ii) to increase of the deficiency at the Si1 sites, and (iii) to introduce conduction electron scattering centers. We have recently found that the Ba deficiency of $Ba_{8-\delta}Si_{46}$ increased at the Ba1 sites upon evacuation at elevated temperatures, and the T_c decreased from 8 K for $Ba_{7.76}Si_{46}$ to 6 K for $Ba_{6.63}Si_{46}$ [16]. The solid solutions of the ternary system studied in this paper have essentially the same Ba occupancy irrespective of the Ge substitution, although there is a slight Ba deficiency in all of the solid solutions. The barium deficiency is not the reason of the decrease of the T_c of the solid solutions. In the early stages of the Ge substitution of $x<13$ in $Ba_{8-\delta}Si_{46-x}Ge_x$, the formation of the deficiency at the Si1 sites is negligible, although the T_c decreases linearly with x. This will be caused by the effects (i) and (iii). Yokoya et al. [11] showed that the superconductivity of $Ba_{8-\delta}Si_{46}$ was driven by a phonon-mediated mechanism. The increase of the lattice constant, i.e. the increase of the covalent bond distances in the network will depress the phonon–electron interaction to form Cooper-pairs. The superconductivity disappeared for the compounds with $x>24$ in the measured temperature range down to 2 K. This will be probably due to the increased deficiency in the (Si, Ge) network at the Si1 sites. The defects at the Si1 sites will trap the conduction electrons and interrupt the conduction path of electrons. The end member $Ba_8Ge_{42.8}$ of this system is a semiconductor.

4. Conclusion

Germanium substituted Type I silicon clathrates $Ba_{8-\delta}Si_{46-x}Ge_x$ ($x<23$) were prepared using high-pressure and high-temperature conditions. The clathrates formed uniform solid solutions, and the lattice constant increased with the increase of the Ge content. All the solid solutions showed superconductivity, and the T_c decreased with the increase of the Ge content. The single-crystal studies revealed the structural effects of the Ge substitution on the bond lengths, site occupancies, and deficiencies in the solid solutions. The structural refinements showed that Ge atoms replaced the Si atoms at the Si3(24*k*) sites in the early stages of the substitution, and then at the Si2(16*i*) sites. The decrease of T_c appears to be caused by the Ge substitution as the effects of the increase of the bond length, the introduction of the conduction electron scattering centers, and the increase of the defects at the Si1 (6*c*) sites.

Acknowledgments

We are grateful to Mr. Yasuhiro Shibata of Hiroshima University for his help in EPMA measurements. This research was partly supported by CREST, Japan Science and Technology Corporation (JST), the COE Research (No. 13CE2002) of the Ministry of Education, Culture, Sports, Science and Technology of Japan, and Electric Technology Research Foundation of Chugoku.

References

[1] S. Yamanaka, H. Horie, H. Nakano, M. Ishikawa, Fullerene Sci. Technol. 3 (1995) 21.
[2] H. Kawaji, H. Horie, H. Yamanaka, M. Ishikawa, Phys. Rev. Lett. 74 (1995) 1427.
[3] J.S. Kasper, P. Hagenmuller, M. Pouchard, C. Cros, Science 150 (1965) 1713.

[4] C. Cros, M. Pouchard, P. Hagenmuller, J. Solid State Chem. 2 (1970) 570.
[5] S. Yamanaka, E. Enishi, H. Fukuoka, M. Yasukawa, Inorg. Chem. 39 (2000) 56.
[6] S. Saito, A. Oshiyama, Phys. Rev. B 51 (1995) 2628.
[7] R.F.W. Herrmann, K. Tanigaki, T. Kawaguchi, S. Kuroshima, O. Zhou, Phys. Rev. B 60 (1999) 13245.
[8] K. Moriguchi, M. Yonemura, A. Shintani, S. Yamanaka, Phys. Rev. B 61 (2000) 9859.
[9] K. Moriguchi, S. Munetoh, A. Shintani, Phys. Rev. B 62 (2000) 7138.
[10] A. Kitano, K. Moriguchi, M. Yonemura, S. Munetoh, A. Shintani, H. Fukuoka, S. Yamanaka, E. Nishibori, M. Takata, M. Sakata, Phys. Rev. B 64 (2001) 45206.
[11] T. Yokoya, A. Fukushima, T. Kiss, K. Kobayashi, S. Shin, K. Moriguchi, A. Shintani, H. Fukuoka, S. Yamanaka, Phys. Rev. B 64 (2001) 172504.
[12] O. Zhou, S. Kuroshima, K. Tanigaki, K. Ishii, H. Suematsu, Proc. Electrochem. Soc. 97-14 (1997) 1180.
[13] W. C-Cabrera, J. Curda, K. Peters, S. Paschen, M. Baenitz, Y. Grin, H.G. Von Schnering, Z. Kristallogr. New Cryst. 215 (2000) 321.
[14] TeXsan: Single Crystal Structure Analysis Software, Ver. 1.6, Molecular Structure Corp. The Woodlands, TN, 77381, 1993.
[15] CrystalStructure 2.00: Crystal Structure Analysis Package, Rigaku and MSC, 2001.
[16] H. Fukuoka, J. Kiyoto, S. Yamanaka, Inorg. Chem. 49 (2003) 2933.